ELSEVIER

Journal of Structural Geology 26 (2004) 1275–1291

JOURNAL OF STRUCTURAL GEOLOGY

www.elsevier.com/locate/jsg

3-D Mohr circle analysis of vein opening, Indarama lode-gold deposit, Zimbabwe: implications for exploration

C.J. McKeagney, C.A. Boulter*, R.J.H. Jolly[1], R.P. Foster[2]

School of Ocean and Earth Science, University of Southampton, Southampton Oceanography Centre, European Way, Southampton SO14 3ZH, UK

Received 31 January 2002; received in revised form 17 November 2002; accepted 2 May 2003

Abstract

The Indarama lode gold deposit is hosted by vertically-dipping basalt in the Late Archaean Midlands Greenstone Belt of Zimbabwe. Major deformation events at 2.68 and 2.58 Ga established a complex array of fractures. A limited range of orientations of this fracture network opened towards the end of the younger deformation event, creating a lode pattern where 92% of mineralised veins dip at less than 50°, mainly to the E and W, and most strike directions are represented. A clustered distribution of poles to the quartz–carbonate veins indicates a constrictional stress field at the time of vein opening where σ_1 and σ_2 were near horizontal, (directed NNW–SSE and ENE–WSW, respectively), and σ_3 was near vertical. 3-D Mohr circle analysis demonstrates that σ_2 was approximately 67% of σ_1 (the stress ratio) and that the driving pressure ratio (R') was approximately 0.4, reflecting the role of fluid pressure, mean stress, and the maximum shear stress in controlling conditions of fracture opening.

Keywords: Veins; Gold; Mineralisation; Stress; Zimbabwe; Fractures

1. Introduction

The Indarama lode gold deposit is part of the Kwekwe gold camp in the Midlands Greenstone Belt, central Zimbabwe. The concentration of gold deposits and their combined production makes the Kwekwe gold camp one of the richest and most productive portions of Archaean crust anywhere in the world in terms of gold yield per square kilometre (Foster et al., 1991). The Indarama mine, which was discovered in 1920 (Macgregor, 1932), has produced over 6 tonnes of gold to date. Gold mineralisation is hosted by homogenous, vertically dipping ca. 2.9–2.7 Ga metabasalts that have been subjected to greenschist facies metamorphism.

The Indarama gold deposit has a relatively simple structural history in comparison with the majority of mesothermal lode gold deposits. Also, the extent of mine workings allows structures to be followed both along strike and down dip in a way that is rarely possible at the surface. The deposit, therefore, provides an opportunity to better understand critical aspects of the mineralisation process, such as the timing relationships of deformation and fluid flow, which are often difficult to resolve elsewhere due to pronounced overprinting by later structural events.

The relative stress and fluid pressure conditions required to open pre-existing fractures at the time of gold emplacement have been assessed using the three-dimensional Mohr-circle construction developed by Jolly and Sanderson (1997). Initially applied to dyke emplacement, the similarity in mechanics of formation of veins and dykes means that this technique is also valid for mineralised veins. Recently there has been much theoretical work relating fluid flow within fracture networks to the stresses acting on them (Barton et al., 1995; Sanderson and Zhang, 1999; Jolly et al., 2000), but there has been less published work in the application of this theory to mineral deposits.

2. Regional geology

The Archaean craton of Zimbabwe covers an area of 650 km by 350 km and is characterised by granite–greenstone terranes in which granitic rocks and greenstone belt remnants constitute 85 and 15% of the craton, respectively (Anhaeusser, 1976). The craton is surrounded by three orogenic belts (Fig. 1a): the Limpopo Belt (2.6–2.0 Ga) to

* Corresponding author. Tel.: +44-23-8059-2670; fax: +44-23-8059-3642.

E-mail address: Clive.A.Boulter@soc.soton.ac.uk (C.A. Boulter).

[1] Present address: Upstream Technology Group, BP Exploration, Chertsey Road, Sunbury-on-Thames, Middlesex TW16 7LN, UK.

[2] Present address: Exploration Consultants Ltd, Highlands Farm, Greys Road, Henley-on-Thames, Oxon RG9 4PR, UK.

0191-8141/$ - see front matter © 2004 Elsevier Ltd. All rights reserved.
doi:10.1016/j.jsg.2003.11.001

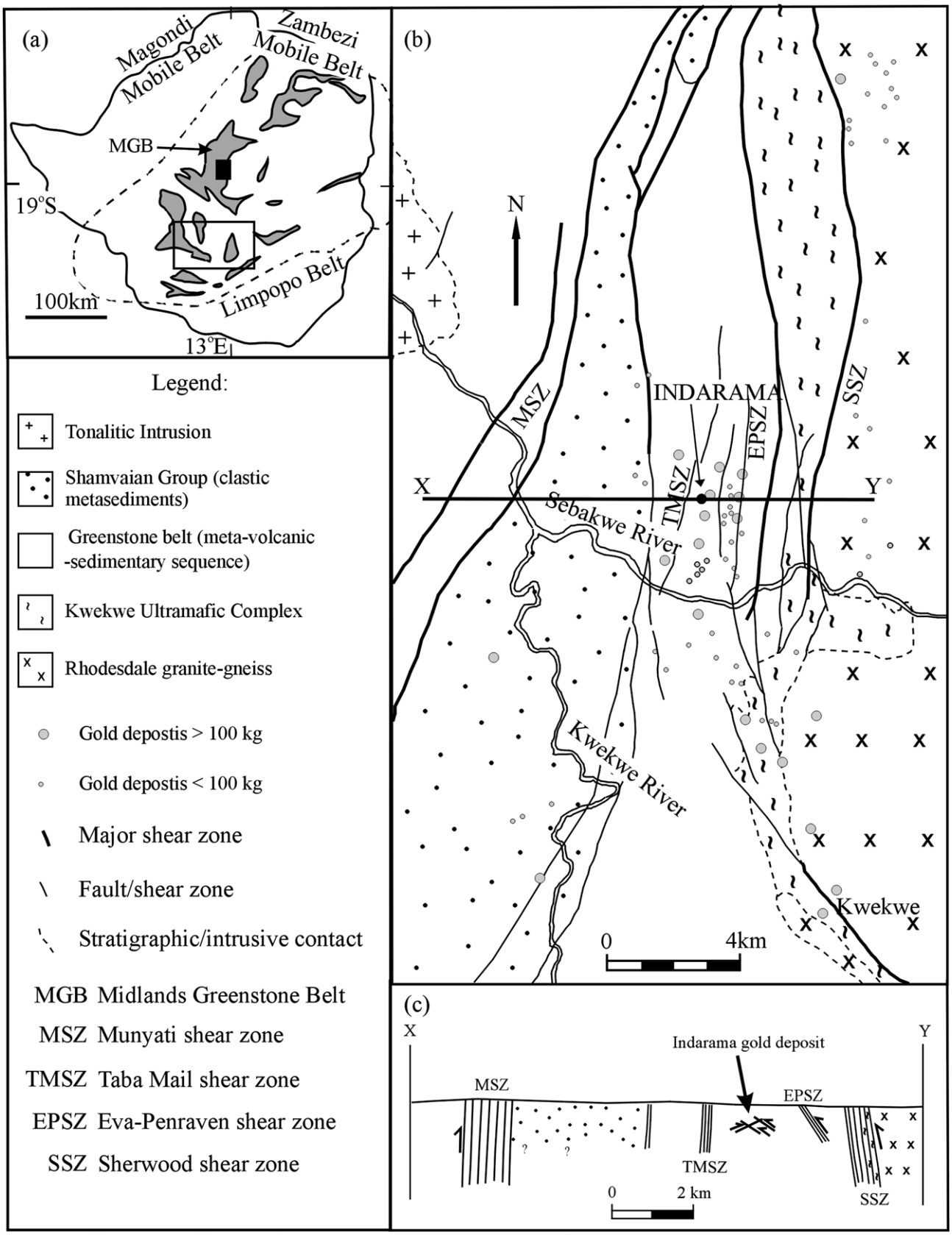

Fig. 1. Regional and district scale setting of the Indarama gold mine. (a) Map of Zimbabwe indicating the extent of the Archaean craton (dashed line), outcrops of Archaean greenstone belts (shaded) and surrounding tectonic belts. Solid rectangle indicates the position of (b). Open rectangle indicates the position of Fig. 3. (b) Regional geology around Indarama Mine (modified after Campbell and Pitfield, 1994). X–Y indicates the line of section in (c). (c) Simplified cross-section through the shear zones of the Midlands Greenstone Belt.

the south, the Magondi Mobile Belt (ca. 2.0–1.8 Ga) to the north and west, and the Zambezi Mobile Belt to the northeast (1.0–0.5 Ga) (Blenkinsop et al., 1997).

The Archaean stratigraphy in Zimbabwe has been documented by various authors (including Macgregor, 1951; Stowe, 1971; Wilson et al., 1978; Nisbet et al., 1981; Wilson, 1981), and more recently summarised by Wilson et al. (1995). Wilson et al. (1978, 1995) and Wilson (1981) correlated the Archaean stratigraphy of Zimbabwe across the craton for a distance of 700 km and determined a stratigraphic model characterised by magma cyclicity beginning with ultramafic–mafic rocks, followed by felsic volcanics and ending with a granitoid event, repeated at least three or four times. Cratonic ages in Zimbabwe vary from ca. 3.6 Ga (Horstwood et al., 1999) to 2.6 Ga (Taylor et al., 1991), with the late Archaean granite–greenstones being more widespread and more varied in composition than those of the early Archaean (Wilson et al., 1995).

The greenstone belts are characterised by steeply dipping sequences and regional-scale folding, and the granite–gneiss terranes show variable deformation. Early models of crustal development involved mainly vertical tectonics (e.g. Macgregor, 1951), but more recent work (e.g. Wilson, 1990; Treloar and Blenkinsop, 1995; Blenkinsop and Frei, 1997; Dirks and Jelsma, 1998) has emphasized the role of wrench and/or accretionary tectonics.

Recent craton-wide tectonic models for Zimbabwe provide a framework for understanding the structural controls on formation of the gold deposits. The tectonic framework of the Midlands Greenstone Belt is dominated by generally N–S-striking shear zones. This fabric was probably determined by E–W compression at 2.68 Ga caused by collision of the Zimbabwe craton with the Motloutse Complex to the SW (Treloar and Blenkinsop, 1995) (Fig. 2a) at the same time as emplacement of the Matok pluton. This collision was synchronous with tectonics to the south of the Zimbabwe craton in which the Central Zone of the Limpopo Belt collided with the Kaapvaal craton of South Africa in a NE–SW direction (Treloar and Blenkinsop, 1995) (Fig. 2a). A phase of continental collision in the Limpopo Belt 100 Ma later involved convergence of the Zimbabwe craton with the Central Zone (and accreted Kaapvaal craton) in a NNW–SSE direction, resulting in thrusting of the Northern Marginal Zone onto the Zimbabwe craton, and associated NNW–SSE crustal shortening across the Zimbabwe craton (Fig. 2b) (Treloar and Blenkinsop, 1995). This collision has been dated at about 2.58 Ga as synchronous with intrusion of the Razi granites (Blenkinsop and Frei, 1997).

Treloar and Blenkinsop (1995) used this model of protracted collisional tectonics across the Limpopo Belt to explain synchronous NNW–SSE directed crustal shortening with approximately NE–SW directed lateral displacement of individual crustal blocks identified in both the Limpopo Belt and the Zimbabwe craton. They identified regional scale strike-slip shear zones consisting of NNE striking sinistral and ESE striking dextral shear zones (Fig. 3) across southern Zimbabwe. These shear zones formed as conjugate sets in response to NNW–SSE directed crustal shortening and provided a mechanism of lateral displacement for the individual crustal blocks, as indicated in Fig. 3.

This pattern of conjugate shear zones and lateral crustal displacement is most clearly observed in Southern Zimbabwe. However, further north in the area around the Midlands Greenstone Belt, the strike-slip tectonics style and lateral displacement of major structural elements, such as the Rhodesdale terrane, are less clear. Lateral displacement of crustal blocks here would have been more complex because the bounding shears of the Rhodesdale terrane (in this area, the Sherwood Shear Zone; Fig. 1b) are orientated at a high angle to conjugate shear zones that accommodated lateral crustal displacement in southern Zimbabwe.

Previous workers (including Stowe, 1980; Foster et al., 1991; Porter and Foster, 1991) have emphasized that compression from the NE (lateral displacement of the Rhodesdale granite–gneiss terrane towards the SW or WSW) was the dominant tectonic control on the formation of gold deposits in the Midlands Greenstone Belt, though at the time there was no constraining craton-wide tectonic model. More recently, Campbell and Pitfield (1994) and Herrington (1995), recognised the importance of NW–SE- or NNW–SSE-directed compression in the formation of gold deposits in the Midlands Greenstone Belt.

3. Midlands Greenstone Belt geology

3.1. Stratigraphy

The Midlands Greenstone Belt is the largest greenstone belt in Zimbabwe (Fig. 1a) and is dominated by a thick volcanic pile of tholeiitic metabasalts that are part of the ca. 2.7 Ga Upper Bulawayan (U2 to U5) of Wilson et al. (1978, 1995). The tholeiitic metabasalts occur as a vertically dipping sequence, striking N–S with exceptionally well preserved pillows and basalt columns indicating a low strain history. These basalts (both massive and pillowed) are the host rocks to the Indarama gold deposit.

The Shamvaian Group (U6 of Wilson et al., 1995) of sedimentary rocks unconformably overlies the greenstone belt volcanics to the west of Indarama Mine (Fig. 1b). The group is dominated by clastic sediments with minor felsic volcanics.

The Rhodesdale granite–gneiss terrane, to the east of the Midlands Greenstone Belt (Fig. 1b) is a composite body including granitic rocks of various ages (Harrison, 1970) but the main body has been dated at ca. 2.9 Ga (Taylor et al., 1991). The Kwekwe Ultramafic Complex of serpentinites and talc–carbonate schists has been tectonically emplaced along the contact of the Midlands Greenstone Belt and the Rhodesdale granite–gneiss complex (Fig. 1b).

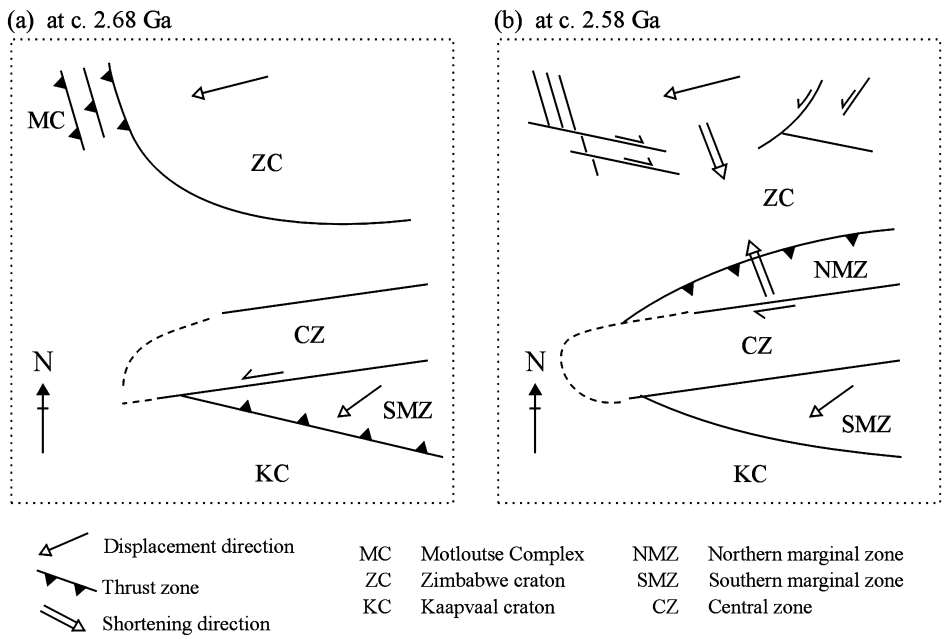

Fig. 2. Schematic diagrams of the nature and timing of deformation in the Limpopo Belt at (a) ca. 2.68 Ga, and (b) ca. 2.58 Ga (modified after Treloar and Blenkinsop, 1995). See text for discussion.

3.2. Structural geology

The structure of the Midlands Greenstone Belt is dominated by regional-scale ductile shear zones and associated second- and third-order brittle faults and shear zones, together with upright folding and granitoid bodies. Campbell and Pitfield (1994) have provided the most recent structural interpretation of the Midlands Greenstone Belt. They concentrated on regional scale observations coupled with outcrop mapping and mine studies at a limited number of localities. From their work, the shear zones of the Midlands Greenstone Belt were defined as an anastomosing array of N- and NNW-trending zones of high to moderate strain, contrasting strongly with the low-strain blocks between. All of the shear zones are sub-vertical except for the Eva–Penraven shear zone, which dips at between 50 and 60° to the east (Fig. 1c).

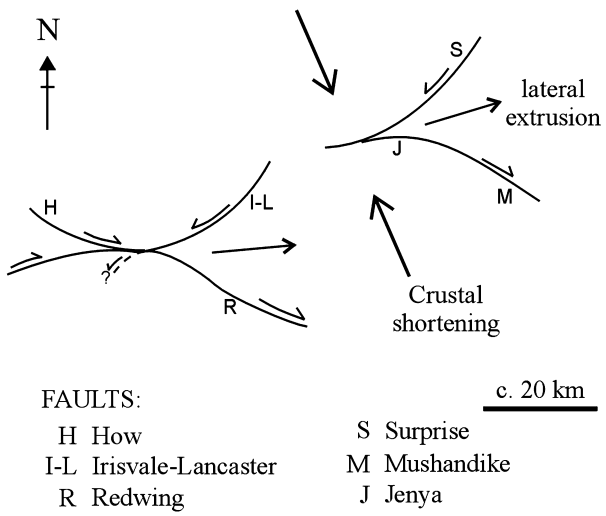

Fig. 3. The conjugate fault system in southern Zimbabwe (modified after Treloar and Blenkinsop, 1995). See Fig. 1a for the location of Fig. 3.

The Sherwood Shear Zone to the east of Indarama, and the Munyati Shear Zone to the west, are generally N- to NNE-striking zones of high to moderate strain developed along the contacts between different rock types (Fig. 1b). The Taba Mali Shear Zone, however, is a poorly defined zone of moderate strain within the Upper Bulawayan metabasalts (Fig. 1b). The shear zones are characterised by a sub-vertical foliation that contains a steeply plunging lineation (Fig. 4) defined by mafic minerals, stretched lapilli, and stretched quartz amygdales. This fabric formed under E–W compression and sub-vertical extension, and in parts has been reactivated in a brittle fashion. In addition, several later generations of steeply-dipping strike-slip faults that trend dominantly N–S with minor E–W striking faults (Fig. 5) have overprinted the foliation. The age and affinity of the E–W brittle faults is poorly constrained, and known only to be post-foliation. Stepped slickenside surfaces and striae on the brittle faults, and reactivated foliation planes, indicate both dextral and sinistral strike-slip displacements on the foliation planes and on the NNE–SSW faults. Where overprinting evidence is available, sinistral displacement was succeeded by dextral reactivation. In contrast the NNW–SSE faults only display sinistral strike-slip indicators suggesting that the NNW striking fault planes were unfavourably oriented during dextral reactivation.

Lateral displacement of the Rhodesdale terrane towards the SW in response to NNW–SSE crustal shortening at ca. 2.58 Ga could have generated both the sinistral and dextral strike-slip displacements along the generally N–S-striking faults and foliation planes in the Sherwood Shear Zone.

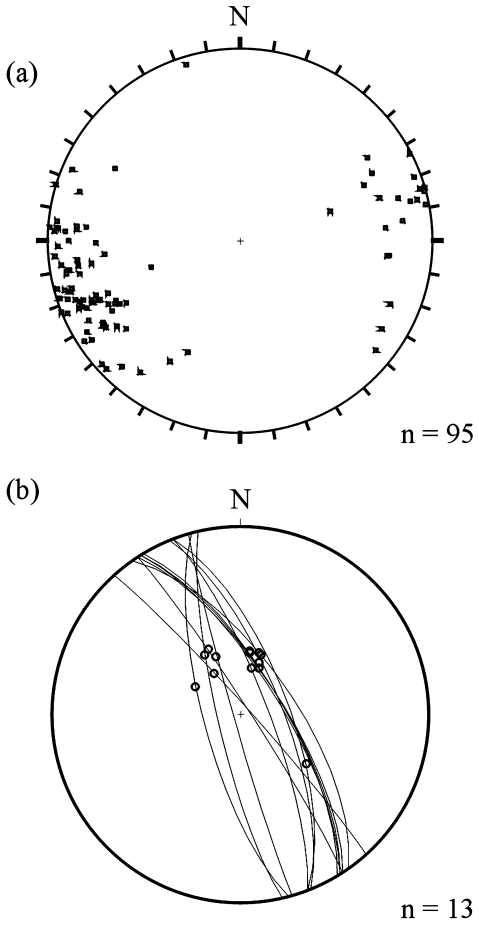

Fig. 4. Foliation and mineral stretching lineation data from the Sherwood Shear Zone (pre-brittle reactivation) plotted on equal-area lower hemisphere stereoplots. (a) Poles to foliation planes. (b) Foliation planes (cyclographic traces) containing stretch lineations (circles).

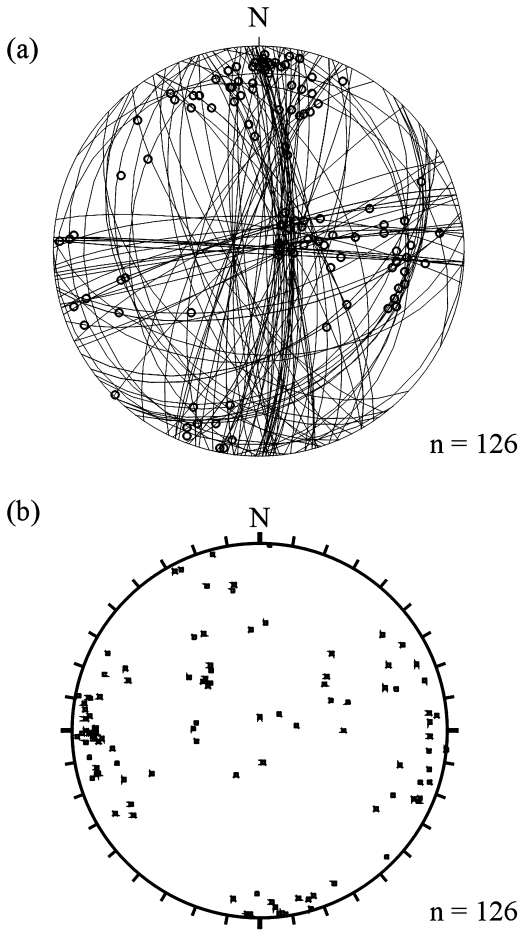

Fig. 5. Foliation planes in the Sherwood Shear Zone that have undergone brittle reactivation (N–S striking) and strike-slip faults developed within the shear zone, equal-area lower hemisphere stereoplots. (a) Cyclographic traces and slickenside striae (circles). (b) Poles to the reactivated foliation planes and strike-slip faults.

4. Indarama mine geology and tectonic evolution

4.1. Introduction

The dominant lodes (orebodies) at Indarama Mine are N–S-striking and dip to the E and W between 25 and 45°; the E-dipping set are the most significant both economically and structurally (Fig. 6). All of the lodes are structurally and petrologically alike, but the main Indarama Lode is the largest orebody, with a strike length of approximately 200 m and down-dip extension of almost 400 m exploited to date. The Indarama Lode dips to the east, with the Benson and Footwall Lodes occurring in its hanging wall and footwall, respectively. The Reverse Lode also strikes N–S and is the only W-dipping lode (Fig. 6). In addition, several minor lodes (only tens of metres in length) occur dipping mainly to the NE.

Individual lodes are typically 1–1.5 m wide and characterised by one or two main veins, commonly 5–15 cm wide, of quartz–calcite (± stibnite), and a discrete enveloping zone of altered metabasalt (Fig. 7a and b). All veins are hybrid veins comprising both shear and extension components in variable proportions indicated by slickenfibres and coarse vein fill, with the shear component dominant in all veins. Episodic fluid flow during repeated veining episodes is indicated by ribbon vein textures, often accentuated by the inclusion of wallrock septa (Fig. 7c and d). Where present, septa are pervasively mineralised and contain higher gold content than both the vein material and adjacent wallrocks. Zones of wallrock alteration are between 20 and 150 cm wide and are characterised by extensive carbonatization and associated bleaching of the metabasalts (Fig. 7a and b). Dense arrays of microveins, composed mainly of calcite with minor chlorite and quartz, are coincident with the zones of alteration (Fig. 7a and b) and probably formed as damage zones around the main veins.

4.2. Alteration and mineralisation

The alteration (gangue) mineral assemblage is dominated by carbonate (mainly ankerite) and chlorite, with sericite and minor quartz. Although alteration varies considerably

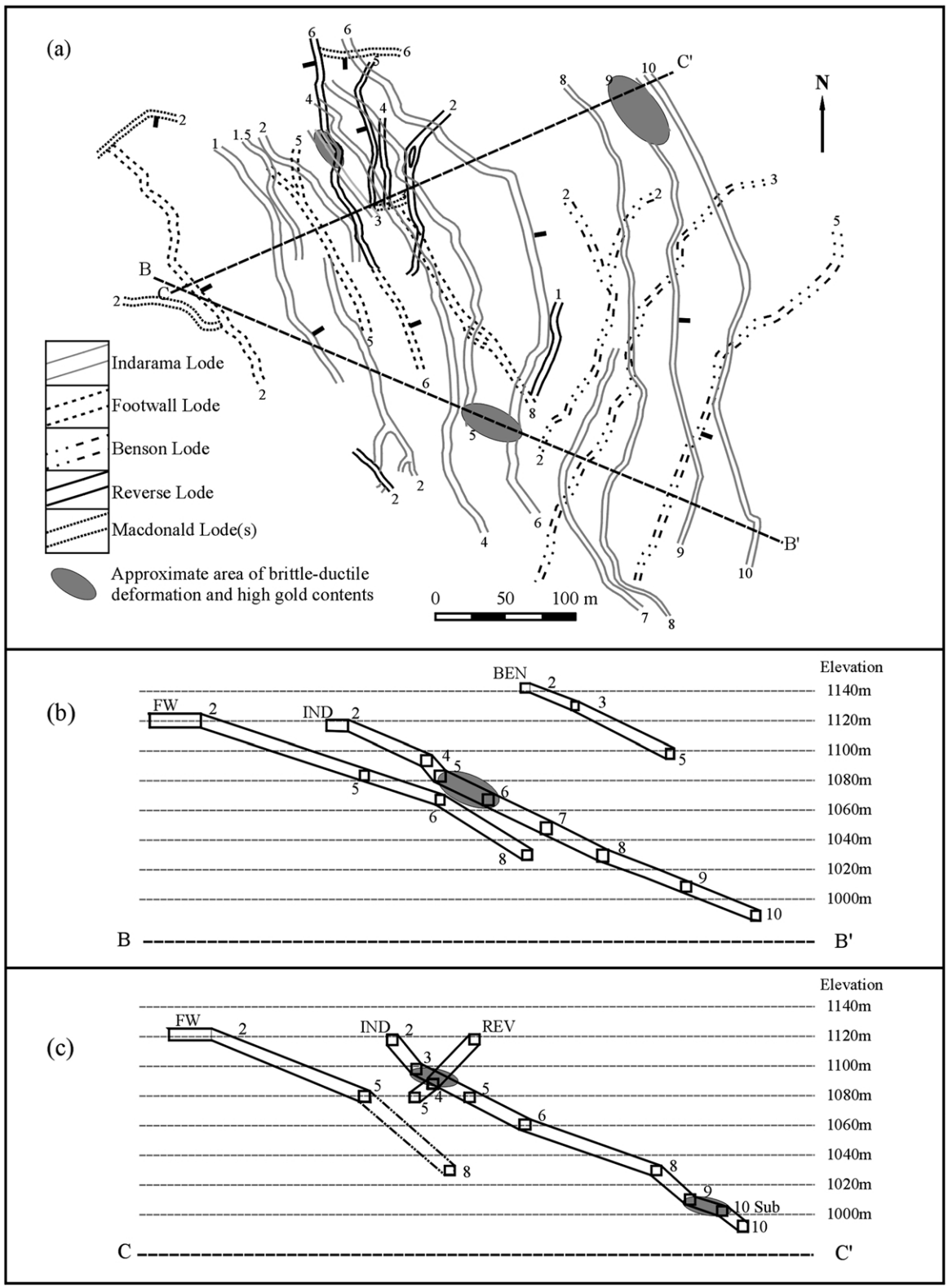
(a)
N
B
B'
C
C'
Indarama Lode
Footwall Lode
Benson Lode
Reverse Lode
Macdonald Lode(s)
Approximate area of brittle-ductile deformation and high gold contents
0 50 100 m
(b)
Elevation
1140m
1120m
1100m
1080m
1060m
1040m
1020m
1000m
FW
IND
BEN
B
B'
(c)
Elevation
FW
IND
REV
10 Sub
C
C'
2 Underground oredrive; figures indicate level of working
Approximate area of brittle-ductile deformation and high gold contents
Lode slightly off the line of section
FW Footwall Lode
IND Indarama Lode
BEN Benson Lode
REV Reverse Lode

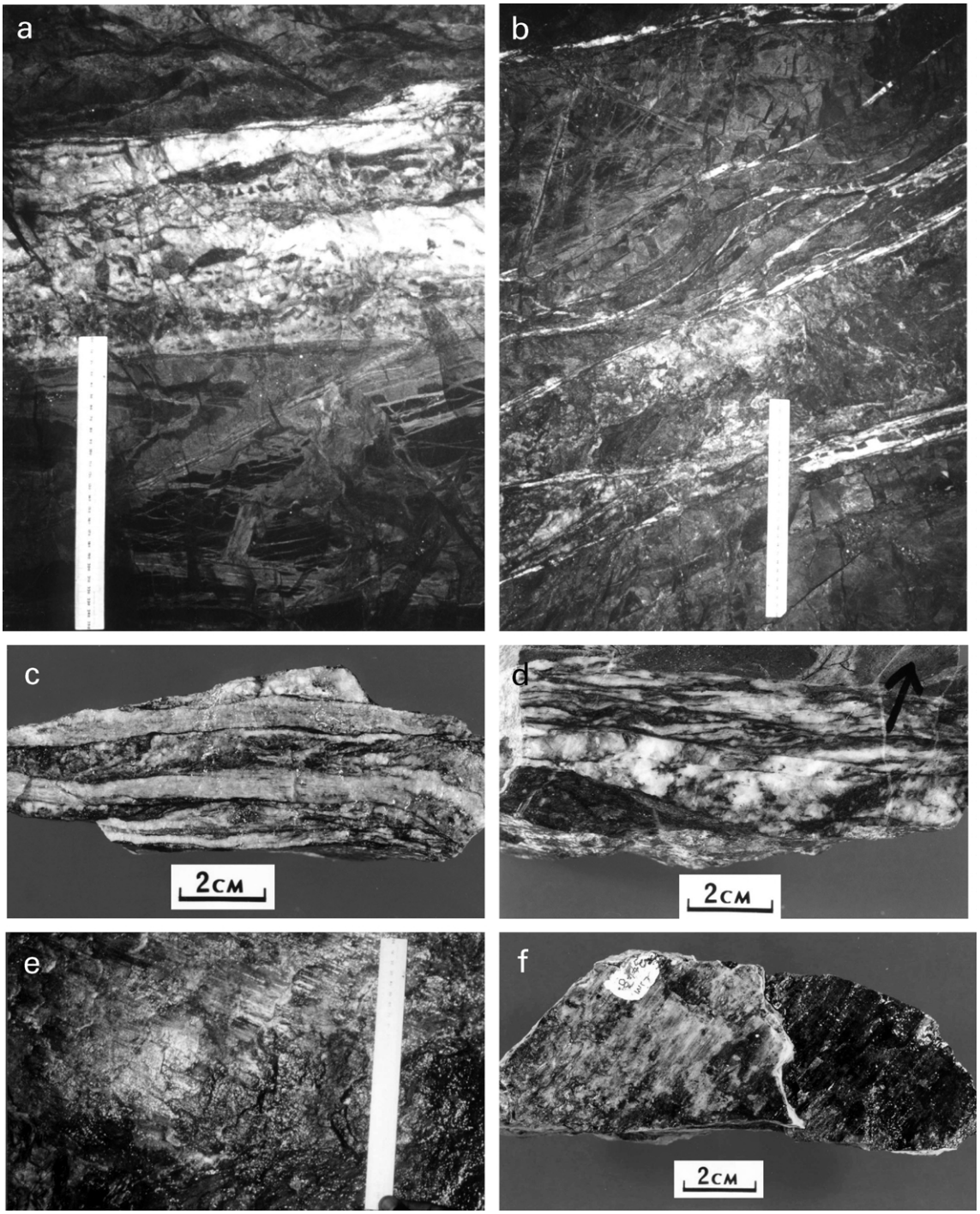

Fig. 7. Deformation features of the main veins of the Indarama and Reverse Lodes. (a) and (b) Main quartz–calcite veins with discrete carbonatized (bleached) haloes of altered basalt around the main vein and microveins, scale = 25 cm: (a) vein dipping 30° towards camera, Reverse Lode and (b) Indarama Lode. (c) and (d) Ribbon quartz shear veins with wallrock septa (Indarama Lode). (e) and (f) Slickenfibre lineations and steps used as kinematic indicators: (e) calcite + stibnite vein, scale = 25 cm and (f) quartz + calcite vein.

Fig. 6. Mine scale setting of individual lodes. (a) Composite level plan of all lodes with ticks to show dip direction; numbers indicate the level of the mine working. (b) and (c) Mine-scale cross-sections along lines BB′ and CC′, respectively, of (a), with elevations in metres above sea level.

locally, a consistent relationship of carbonate overprinting chlorite/chlorite–sericite is apparent. Sulphide mineralisation, mainly in the form of pyrite disseminated through the metabasalt wallrock, within microveins, and at vein–wallrock contacts, is spatially associated with host rock carbonatization, and calcite and chlorite microveining. Repetitions of the same alteration assemblage occurred cyclically associated with successive pulses of hydrothermal activity during repeated fracturing along the main veins. Analogous to the silicate alteration, there were multiple generations of sulphide mineralisation, but a distinctive paragenetic sequence has not been identified, instead repetitions of the same sulphide mineral assemblage are evident.

4.3. Kinematics and geometry

Kinematic indicators used include slickenfibres, stepped slickensides (Fig. 7e and f), dilational jogs (Fig. 8) and S–C fabrics in the brittle–ductile regions. Slip lineations in the main veins of all of the lodes consistently pitch at high angles (Fig. 9), with alternations of reverse-sinistral and reverse-dextral slip being common. These have the overall effect of reverse dip-slip movement with limited displacement (decimetres to metres scale displacements). Where the chronological order of overprinting slickenfibre lineations is clearly apparent, variations in slip vectors suggest only slight and/or gradual changes in slip direction, giving an overall sense of displacement that varies around reverse dip-slip with both dextral and sinistral components (Fig. 10). The chronological order of slip events recorded by slip lineations cannot be correlated along any lode, or from one lode to another, but a consistent pattern of alternating reverse-sinistral and reverse-dextral displacements is clearly apparent in the main veins of all lodes.

The E and W dipping lodes define a conjugate pair of shallowly dipping, reverse sense shear zones. Their conjugate relationship is indicated by the average slip lineations occurring close to the intersections of the veins

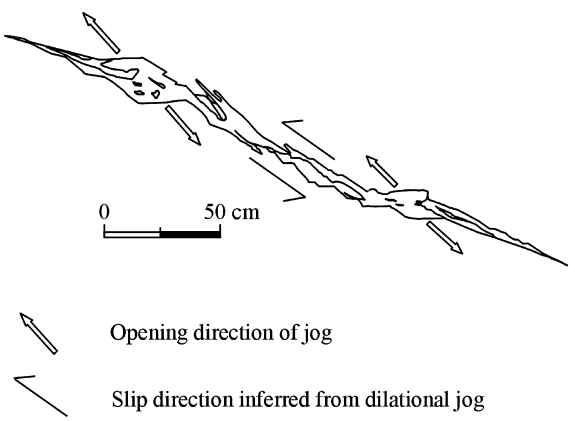

Fig. 8. Field sketch (facing north) of dilational jogs in the main veins of the Indarama Lode, 5 level north (vertical face). Shear sense along the vein is determined from jog geometry and opening direction.

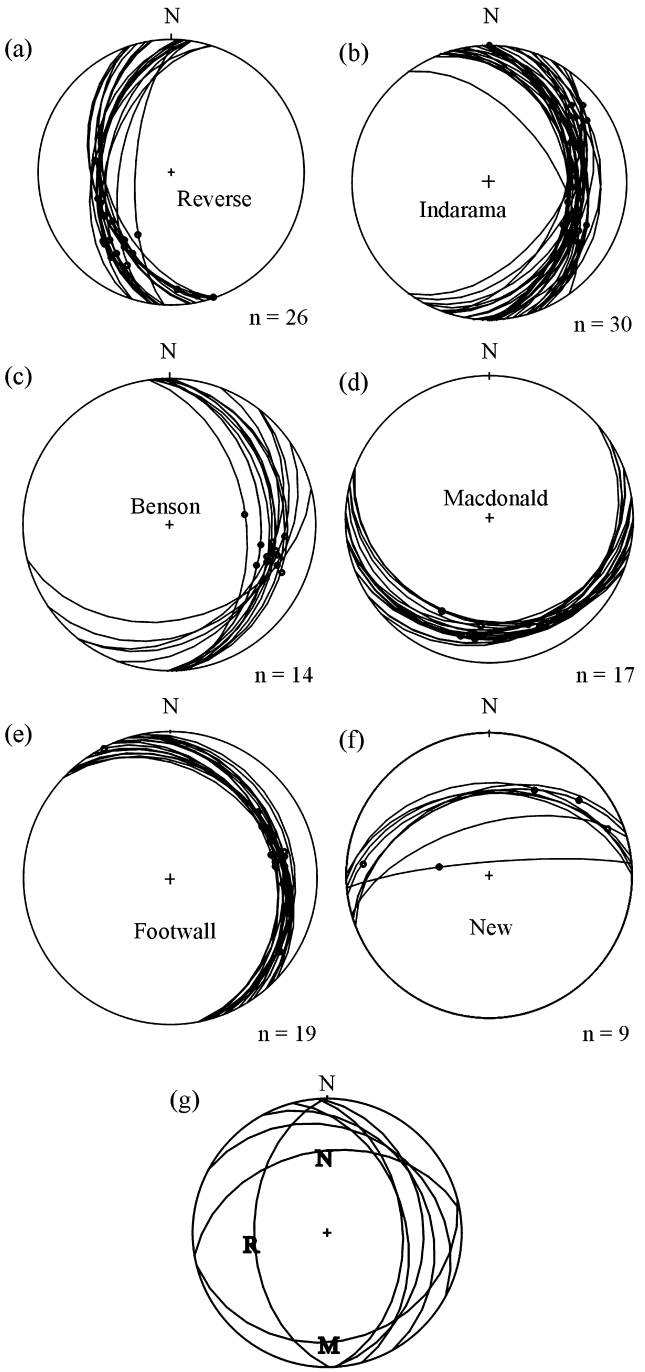

Fig. 9. Equal-area lower hemisphere stereoplots of main veins (cyclographic traces) and slip lineations (circles) for all the exploited lodes ((a)–(f)). (g) Cyclographic traces representing average orientations of all the Lodes (N = New Lode, R = Reverse Lode, M = Macdonald Lode).

with the profile plane (Fig. 11a), a dihedral angle of 60°, and mutual offsets of the structures on all scales; this is seen particularly well on 2 level, drive south, at the intersection of the Indarama and Reverse Lodes where minor veins (1–4 mm wide) parallel to the main Indarama and Reverse Lodes show mutual offsets all in a reverse sense (Fig. 11c). At this intersection, both lodes pinch out to the south with a complex array of splays of the Indarama Lode.

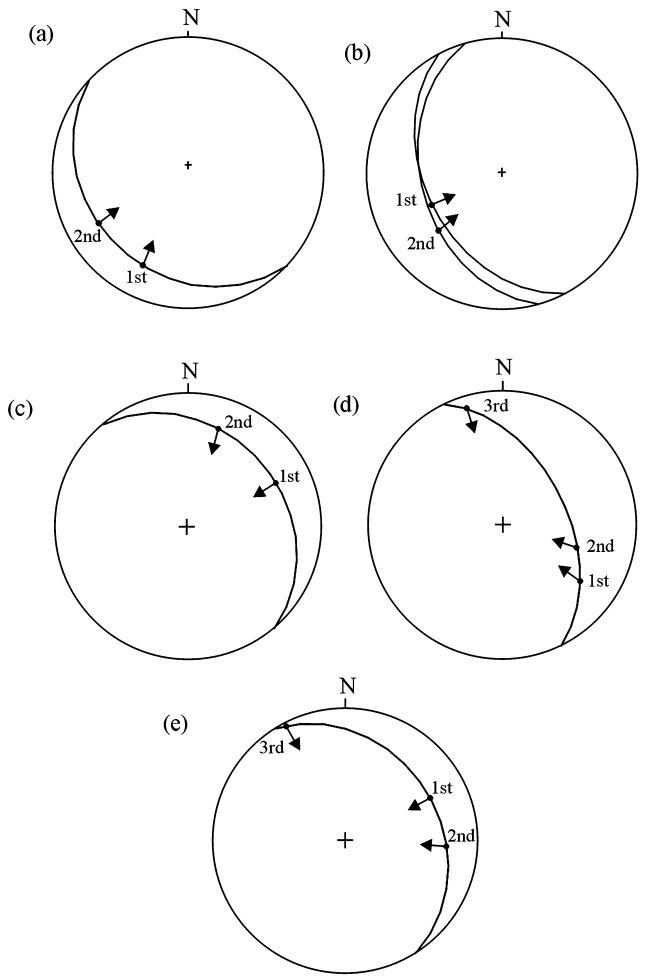

Fig. 10. Relative timing of cross-cutting slip lineations. (a) and (b) Reverse Lode, 5 level. (c)–(e) Footwall Lode, 5 and 6 Levels. Arrows indicate hanging wall movement.

The N and S dipping lodes (New and Macdonald Lodes) are structurally, mineralogically and texturally the same as the E and W dipping lodes (Indarama, Footwall, Benson and Reverse Lodes), including the range of reverse dip-slip to reverse oblique-slip displacements (although relatively little kinematic data was observed on the New Lode) and therefore the same structural history is assumed. There is no evidence to suggest a different genetic interpretation of the N and S dipping lodes, and it is possible that they also constitute a conjugate pair, subordinate to the dominant E and W dipping conjugate lodes. The synchroneity of the N and S dipping lodes with the main E and W dipping lodes is indicated on 5 and 6 levels, north. On 5 level, the New Lode (N dipping) has been offset 5 m (sinistrally) by the Indarama Lode (E dipping), and on 6 level, the New Lode displaces the Reverse Lode (W dipping) by 2 m (reverse sinistral).

Field and petrological evidence indicates that the veins hosting the lodes at Indarama dilated synchronously; cross-cutting relationships, identical ore and alteration assemblages, veining episodes, and mutual offsets of lodes, suggest veining and alteration were synchronous and repetitive in all lodes. The conjugate nature of the E- and W-dipping lodes is explained by the stress field illustrated in Fig. 11a, with sub-horizontal ENE–WSW-directed σ_1 (maximum compressive stress) and NNW–SSE-directed σ_2, and a sub-vertical σ_3 (minimum compressive stress). Taking into account the subsidiary lodes of varying strike orientations, including the Macdonald, New and various spur lodes, all of which are reverse structures, additional compression to σ_1 from the ENE must have been acting on the area to produce reverse structures that vary so much in orientations. All of the lodes share a common sub-vertical extension direction, σ_3, and therefore the intermediate principal stress σ_2 (NNW–SSE) was compressional and similar in magnitude to σ_1, with the effect of producing constrictional horizontal compression in an oblate stress ellipsoid. Indeed it is likely that σ_1 and σ_2 switched several times during vein reactivation at Indarama with the dominant compression direction alternating between ENE–WSW and SSE–NNW.

4.4. Brittle–ductile deformation

Although deformation is dominated by brittle structural elements (veining and microveining) brittle–ductile deformation was noted in three localities in the mine. These brittle–ductile parts of the lodes are only metres in extent but they contain gold grades an order of magnitude higher than adjacent areas of brittle deformation (up to 36 ppm between 5 and 6 levels south of the Indarama Lode; Fig. 6b). The positions of these three localised areas of brittle–ductile deformation are indicated on Fig. 6. In these areas, fluid access was greatly increased by increasing vein apertures at mine scale lode intersections (Fig. 6b near convergence of Indarama and Footwall Lodes between 5 and 6 levels; Fig. 6c intersection of Indarama and Reverse Lodes, 3 to 4 levels) and at a mine scale dilational jog (Fig. 6c shallowing of Indarama Lode between 9 and 10 levels). Numerical modelling has indicated that when fracture intersections are opened the rate of fluid flow through the fracture network changes abruptly to become highly localised (Zhang and Sanderson, 1997). This modelling of the mechanical and hydraulic behaviour of rocks has been quantified and shows that flow rates along fractures with lengths much greater than their aperture thickness (such as fractures at Indarama) are determined using the cubic law, according to which an increase in fracture aperture will increase the rate of flow by a power of three (Zhang and Sanderson, 1997). The resultant increase in fluid flow rate at these lode intersections and dilational jogs, therefore, greatly increased the extent of fluid–rock interaction and hence alteration. The locally enhanced alteration of basalt to mica, sericite and chlorite at these localities resulted in a greater proportion of weaker minerals and a consequent change in the host rock rheology permitting brittle–ductile rather than brittle deformation. It is presumed that these

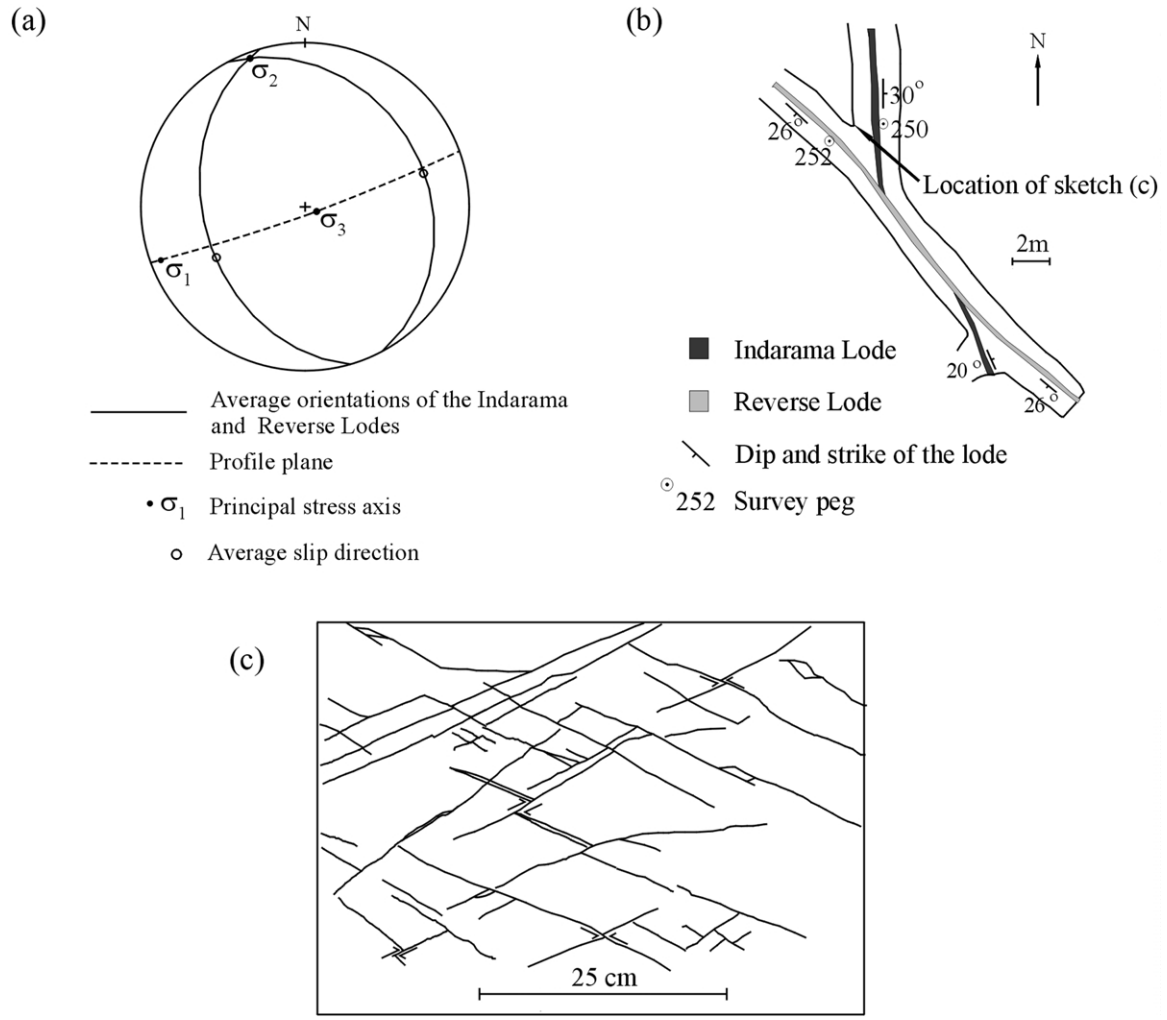

Fig. 11. (a) Conjugate model of the main E- and W-dipping lodes. Average orientations of the main veins and slip lineations taken from data on all levels of the mine. (b) Oredrive plan of the Indarama and Reverse Lodes, 2 level south. (c) Field sketch of minor veins parallel to the main veins of the Indarama and Reverse Lodes showing mutual offsets (facing 320°).

brittle–ductile areas were sites of enhanced fracture densities which facilitated intensive wallrock alteration.

4.5. Formation of the Indarama gold deposit in the context of regional tectonics

Viewing the total lode data, the comparable dips of the majority of veins, and the broad range of strikes, indicates qualitatively that σ_2 was similar in magnitude to σ_1 during vein opening, i.e. an oblate stress ellipsoid. The maximum (σ_1) and intermediate (σ_2) principal stresses were determined to be sub-horizontal with σ_1 orientated ENE–WSW, and σ_2 NNW–SSE (Fig. 11a). Interchanging of the orientations between the maximum and intermediate principal stresses explains the alternations of reverse-sinistral and reverse-dextral slip increments recorded on the veins and the sinistral and dextral reactivations of the regional shear zones. These alternations of dominant compression from the ENE and SSE would have a long-term effect of protracted application of a horizontal constrictional stress field.

The orientation of this local tectonic stress field acting at the time of vein reactivation and gold mineralization at Indarama is compatible with regional tectonics (NNW–SSE crustal shortening, and ENE–WSW lateral crustal displacement) at ca. 2.58 Ga (Fig. 2b).

5. Mohr circle analysis of vein opening

The structures within the Midlands Greenstone Belt in the vicinity of Indarama Mine have been ascribed to two distinct craton-wide deformation episodes (Fig. 2) and are dominated by the N–S striking shear zones (Fig. 1b). Joints and microfaults were created during the formation of the N–S shear zone array as well as during several deformation phases that reactivated and overprinted the shear zone fabrics. Of these the mineralised veins are the best defined structural elements in the basalt sequence but they probably

represent only a proportion of the brittle structures developed up to the time of deposit formation. The following analysis concentrates on the dilation event(s) that allowed auriferous fluid to flow through the rock mass and to react with the basalt via a surface area that was much enhanced by the microfractured damage zones around the main veins.

5.1. Theoretical basis

The R ratio was devised by Delaney et al. (1986) to carry out a 2-D investigation of the stress conditions under which dykes were emplaced into older fractures. These authors studied dykes intruded into undeformed sedimentary rocks on the Colorado Plateau in order to determine a driving stress for dilation. They determined that, for a fracture to be opened by a fluid, the fluid pressure (P_f) must equal or exceed the normal stress (σ_n) acting on the fracture. By combining the normal stress and fluid pressure parameters, conditions for fracture opening can be expressed as Eq. (1). In doing this, Delaney et al. (1986) introduced the R ratio (Eq. (2)) as a means to determine which fracture orientations can dilate in a stress regime:

$$P_f \geq \frac{\sigma_{max} + \sigma_{min}}{2} + \frac{\sigma_{max} - \sigma_{min}}{2}\cos 2\theta \quad (1)$$

$$R = \frac{P_f - \dfrac{\sigma_{max} + \sigma_{min}}{2}}{\dfrac{\sigma_{max} - \sigma_{min}}{2}} = \frac{P_f - \sigma_m}{\tau_{max}} \geq \cos 2\theta \quad (2)$$

where σ_{max} and σ_{min} are the maximum and minimum principal stress, respectively, τ_{max} is the maximum shear stress and σ_m is the mean stress. The angle between the normal to the fracture and the maximum principal stress (θ) defines the ranges of orientations of fractures that can dilate under a given fluid pressure (P_f). Delaney et al. (1986) called this R ratio the *driving stress ratio*.

In order to assist the analysis of fluids opening fractures, Jolly and Sanderson (1997) plotted fluid pressure on the Mohr circle as the value of the normal stress based on the principle that the limit of dilation is where $P_f = \sigma_n$. A vertical line locating the fluid pressure (at $P_f = \sigma_n$) divides the Mohr circle into two fields—fractures able to dilate because $P_f \geq \sigma_n$ and fractures that will remain closed where $P_f \leq \sigma_n$. This construction provides a useful tool to visually represent the range of fracture orientations that will open in a given stress state.

The 2-D representation of stress on Mohr circles can easily be extended to three dimensions (e.g. Means, 1976; Jaeger and Cook, 1979), where three orthogonal principal axes of stress are considered: maximum (σ_1), intermediate (σ_2) and minimum (σ_3). Compression is taken to be positive. A 3-D Mohr diagram includes three circles corresponding to the σ_1–σ_2, σ_1–σ_3 and σ_2–σ_3 planes, and the state of stress on any other plane plots in between the circles. The R ratio for 2-D stress analysis of Delaney et al. (1986) has been extended to three dimensions by Baer et al. (1994) by introducing two new terms to further describe the state of stress and fluid pressure, namely the stress ratio (ϕ) and the driving pressure ratio (R'). The stress ratio, ϕ (Eq. (3)), indicates the shape of the stress ellipsoid by describing σ_2 with respect to σ_1 and σ_3 (Angelier, 1984; Baer et al., 1994):

$$\phi = \frac{\sigma_2 - \sigma_3}{\sigma_1 - \sigma_3} \quad (3)$$

The stress ratio varies from $\phi = 0$ to $\phi = 1$; a lower ϕ value indicates a prolate stress ellipsoid where σ_2 is closer in magnitude to σ_3 than σ_1. The stress ratio (ϕ) increases as σ_2 moves closer in magnitude to σ_1, producing an oblate stress ellipsoid.

Whereas the stress ratio (ϕ) describes the magnitude of σ_2 relative to σ_1 and σ_3, the driving pressure ratio, R' (Eq. (4)) describes the magnitude of the fluid pressure compared with σ_1 and σ_3 (Baer et al., 1994; Jolly and Sanderson, 1997):

$$R' = \frac{P_f - \sigma_3}{\sigma_1 - \sigma_3} \quad (4)$$

The driving pressure ratio R' varies in value from $R' = 0$ when fluid pressure is equal to the minimum stress ($P_f = \sigma_3$), to $R' = 1$ when $P_f = \sigma_1$. The R ratio of Delaney et al. (1986) differs from the R' of Baer et al. (1994) in its characterisation of P_f; the R ratio compares P_f with mean stress whereas R' compares P_f with σ_3 (Eq. (4)).

Jolly and Sanderson (1997) illustrated how the range of fractures able to dilate in a particular stress state can be transferred from a 3-D Mohr circle to a stereographic projection. Measuring 2θ (twice the angle between the pole (normal) to a vein and the maximum stress) on a Mohr circle, allows the field of fractures able to dilate to be constructed on a stereographic projection. When P_f is less than σ_2, the poles to fractures able to dilate define a cluster distribution around σ_3, whereas when P_f is greater than σ_2, poles to fractures able to dilate form a girdle distribution perpendicular to σ_1. Applying this principle to a whole range of theoretically possible fluid pressures, with an increase in fluid pressure the range of fractures able to dilate expands from a small cluster around σ_3 to a girdle distribution perpendicular to σ_1, until all fractures are able to dilate when $P_f = \sigma_1$.

The relationships explained above use the relative magnitudes of stresses and fluid pressure (on a Mohr circle) to predict the range of fracture orientations able to dilate. This principle can be inverted, using the distribution of vein or dyke data on a stereogram to determine the relative values of stress and fluid pressure on a Mohr circle, thereby providing information on the stresses controlling fracture opening (reactivation).

When the fluid pressure exceeds the tensile strength of

the rock mass plus the minimum stress new fractures will propagate. A rock mass with a high tensile strength will favour the exploitation of pre-existing fractures over propagation. Jolly and Sanderson (1997) used the above method on dykes, and their data illustrated fluid pressure states of $\sigma_3 < P_f < \sigma_2$ and $\sigma_3 < \sigma_2 < P_f$, i.e. cluster and girdle distributions of data, respectively. In their example, magma pressure was demonstrated to have exceeded σ_2 in the case of the gabbro dykes. As the stress ratio, ϕ (Eq. (3)), tends to zero, there is an increased likelihood that the intermediate stress (σ_2) will be exceeded by the fluid pressure before the tensile strength of the rock mass.

5.2. Application of Mohr circle analysis of vein opening to Indarama

From the analysis presented earlier, which highlighted mutual overprinting, identical ore and alteration mineral assemblages, and a consistent deformation pattern of the lodes, it is believed that all the fractures that now host the main shear veins were able to dilate synchronously. Therefore, the vein geometry appears amenable to analysis by the Mohr circle construction developed by Jolly and Sanderson (1997) to determine the stresses and fluid pressures that controlled vein opening, and hence gold mineralisation at Indarama. The contemporaneous nature of the veins rules out the alternative interpretation of several discrete vein-forming deformation episodes. If this latter model were valid, the N and S dipping lodes (New and Macdonald Lodes; Fig. 9d and f), because of their reduced dihedral angle, could potentially be viewed as being initiated as hybrid fractures that dilated as they grew (e.g. Hancock, 1985; Nguyen et al., 1998). However, such an interpretation is not sustained because of the mutual overprinting between all lode sets where other pairings of lodes have dihedral angles of around 60° (e.g. Indarama and Reverse; Figs. 9a and b and 11a). Any dilation on these lodes would have to be generated by a rideover-type of mechanism (Hodgson, 1989), which is unlikely given the very limited slip documented.

Orientation data are presented from the main veins only of all lodes (Fig. 12a). These are distinguished from microveins by scale—all veins greater than 0.5 cm in width have been included in this analysis. The microveins within the wallrocks of the main veins are, therefore, not included. When the total orientation data for the veins that define all of the lodes are displayed, it is clear that almost all possible strike orientations are present. The great majority of poles to veins plot around the centre of the stereonet, steep dips are very rare, and lower dips are evident for the southerly dipping veins (Macdonald Lode; Fig. 12b). This results in a cluster distribution of poles to veins rather than a girdle distribution (Mardia, 1972; Woodcock and Naylor, 1983). The centre of the cluster will define σ_3 because poles to dilated fractures are expected to cluster around the minimum principal stress and all of the lodes share a common sub-vertical extension direction.

As fluid pressure increases within a rock mass containing a range of orientations of fractures the first deformation that occurs is shearing of suitably oriented fractures (Phillips, 1972). As the fluid pressure increases further it will eventually exceed the normal stress acting on fracture walls of a certain orientation resulting in dilation (Delaney et al., 1986). The focus of this paper is on the dilation phase of deformation where vein fill preserves the dilational deformation. It is likely that many fractures within the Indarama rock have undergone shear deformation as well. This analysis therefore considers only part of the total deformation of the Indarama rock mass.

Poles to pure extension veins would form a tight cluster around σ_3. However, poles to veins at Indarama form a scatter around σ_3 reflecting reactivation of pre-existing fractures rather than propagation of new fractures. This in turn reflects the relationship of fluid pressure to σ_3, to the tensile strength of the rock (T), and to the tensile strength of the fractures (T_f). The fractures at Indarama had a low tensile strength due to hydrothermal sealing by veins. This low tensile (cohesive) strength was significantly lower than the tensile strength of the massive basalt host rock. The presence of veins indicates that fluid pressure did exceed σ_3; however, the spread of data and field observations indicate that new tension veins did not form, instead pre-existing fractures were reactivated (repeatedly) and therefore fluid pressure did exceed $\sigma_3 + T_f$ but did not exceed $\sigma_3 + T$.

The cluster (as opposed to girdle) distribution of the main veins (Fig. 12) is characteristic of situations where the poles to dilated fractures plot around σ_3 and where the fluid pressure is less than σ_2 (Jolly and Sanderson, 1997). Therefore, the least principal stress, σ_3, at the centre of the cluster, has a plunge of 82°. The plane of symmetry through the long axis of the elliptical distribution of lodes has been taken as being the σ_2–σ_3 plane, because a greater spread of lodes is to be expected on the σ_2–σ_3 plane where fracture opening is easier against σ_2 rather than σ_1; this distribution would expand if P_f approached the value of σ_2. This locates σ_1 as the pole to the plane of symmetry through the long axis of the elliptical distribution of lodes. The orientations of the principal stress axes shown on Fig. 12c and d will be used to determine the relative magnitudes of principal stresses and fluid pressure during vein reactivation and mineralisation at Indarama.

The ellipse drawn on Fig. 12d (shaded) includes all vein data within the 1% contour (Fig. 12c) and contains 92% of the vein data, with the remainder being very dispersed. The ellipse is taken as dividing the stereogram into two fields—within the ellipse are poles to fractures that have dilated (veins), and outside the ellipse fractures are assumed to have been unable to dilate by P_f overcoming σ_n. Instead, the veins outside the ellipse are considered to represent fractures dilated

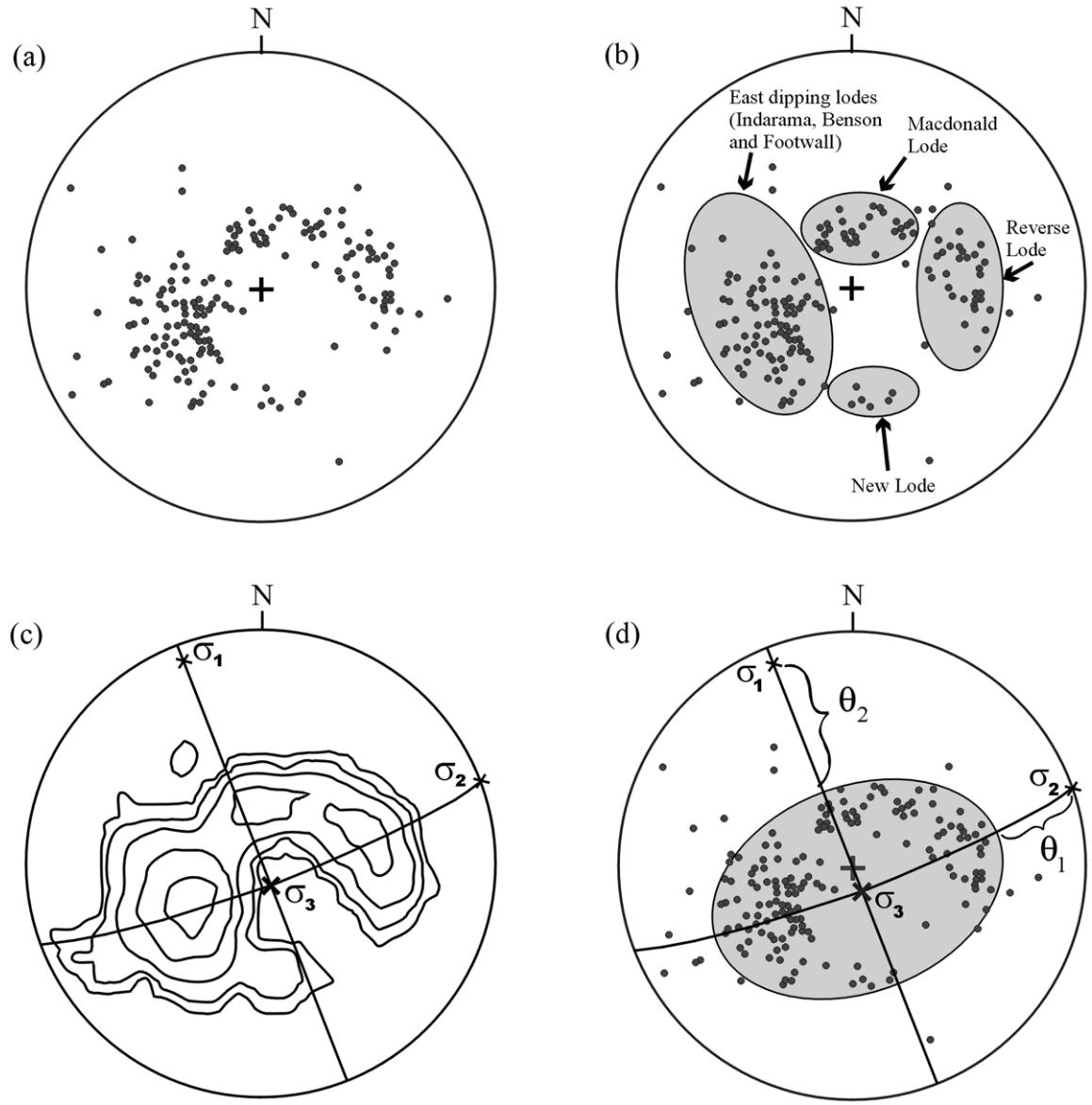

Fig. 12. (a) Equal-area lower hemisphere stereoplots of poles to 187 main veins from all lodes. (b) Same as (a) with lode names superimposed on clusters of poles to veins. (c) Contoured version of part (a); contours at 1, 2, 4, 8 and 16% per 1% area. The least principal stress (σ_3) was located in the centre of the elliptical distribution defined by the contour pattern. The σ_2–σ_3 plane is taken to be the long axis of this elliptical distribution and the σ_1–σ_3 plane is perpendicular to σ_2. (d) The shaded ellipse was constructed to include all vein data within the 1% contour of (c)—concentrations lower than this are not considered significant in the analysis of vein opening; the shaded area indicates the range of fracture orientations that fluid pressure was able to dilate. The angles θ_1 and θ_2 allow the 3-D Mohr circle (Fig. 13) to be constructed.

because of movement constraints placed on local fracture-defined blocks causing local perturbations in the stress field rather than being dictated by the regional fluid pressure and stress regime. The ellipse is centred on the σ_3 axis and is symmetrical around this axis indicating the range of fracture orientations around σ_3 that could dilate. Using the principal stress axes indicated in Fig. 12c, θ angles were measured on the stereogram between the edge of the ellipse and the principal stress axes. θ_2 measured in the σ_1–σ_3 plane is 50°, and θ_1 measured in the σ_2–σ_3 plane is 38° (Fig. 12d). These values of θ_1 and θ_2 were entered into Eqs (3) and (4) to determine the stress ratio (ϕ) and the driving pressure ratio (R') as follows:

Stress ratio:

$$\phi = \frac{\sigma_2 - \sigma_3}{\sigma_1 - \sigma_3} = \frac{1 + \cos 2\theta_2}{1 + \cos 2\theta_1} = \frac{1 + \cos 100}{1 + \cos 76} = 0.67 \quad (5)$$

Driving pressure ratio:

$$R' = \frac{P_f - \sigma_3}{\sigma_1 - \sigma_3} = \frac{1 + \cos 2\theta_2}{2} = \frac{1 + \cos 100}{2} = 0.41 \quad (6)$$

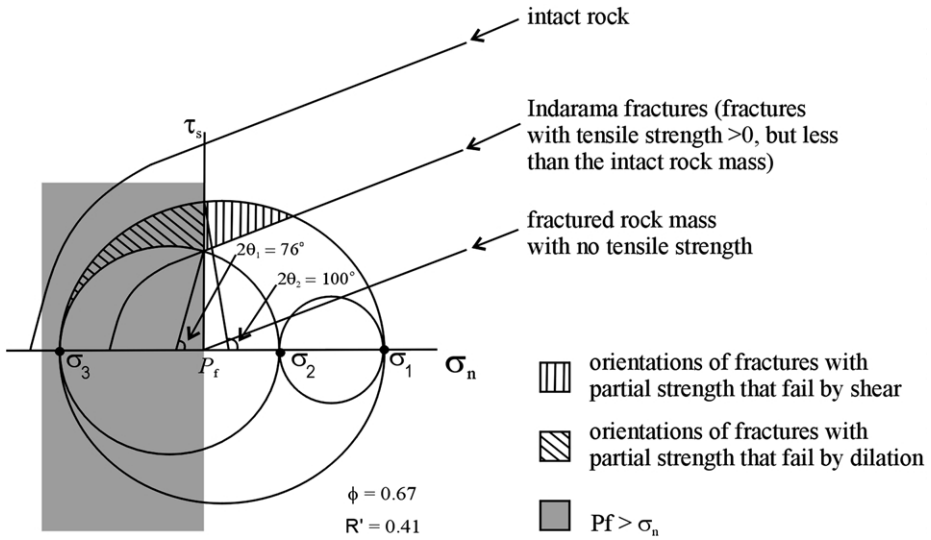

Fig. 13. The 3-D Mohr circle constructed for Indarama vein data from Fig. 12. The stress ratio is 0.67, the driving pressure ratio is 0.41. The shaded area represents the relationship of P_f to the principal stresses in general, and the hatched areas represent orientations of fractures that undergo dilation and shear within the Indarama stress regime.

These values of $\phi = 0.67$ and $R' = 0.41$ were then used to construct the Mohr circle shown in Fig. 13. Once the Mohr circle was constructed, the 2θ angles of $2\theta_1 = 76°$ and $2\theta_2 = 100°$ were included to confirm the location of the P_f ($= \sigma_n$) line.

5.3. Fluid pressure cycling considerations

Sibson and various other workers (Sibson, 1985, 1992, 2001; Sibson et al., 1988; Nguyen et al., 1998; Cox et al., 2001) describe a fault-valve action and associated cyclic fluctuations in fluid pressure within faults as an important mechanism in the formation of mesothermal lode gold deposits. In this structural cycle Sibson et al. (1988) envisage a prefailure stage during which fluid pressure builds up and fault veins remain sealed. This is followed by fault failure when fluid pressure overcomes the stresses acting on the fault, and post-failure discharge accompanied by a consequent drop in fluid pressure. Fault sealing by hydrothermal deposition ends the cycle, providing conditions for a build up of fluid pressure and repetition of the cycle.

Many features of these mesothermal lode gold deposits described by Sibson et al. (1988) are also characteristic of the Indarama lode gold deposit, including a tholeiitic basalt host rock metamorphosed under low- to mid-greenschist facies conditions, gold-bearing quartz veining occurring late in the deformation history, a deformation style of reverse-sense oblique shearing with repeated sealing and reactivation, and carbonatization of the surrounding host rock. The major difference between these typical mesothermal lode gold deposits and the Indarama deposit is the orientation of the shear veins. Sibson and co-workers describe *fault veins* that are steeply dipping (50–80°) reverse faults with associated sub-horizontal extension veins (*flats*), whereas the fault veins at Indarama dip at ca. 30° and there are no sub-horizontal extension veins. Even the shallowest veins at Indarama in the Macdonald Lode (15–20° dips) are reverse-oblique shear zones. The obvious implication of this difference is that the large increases in fluid pressure required to reactivate faults that are unfavourably orientated (i.e. high angle reverse faults) are not required to reactivate the faults at Indarama, which, dipping at ca. 30°, are ideally orientated for reactivation in a stress regime of horizontal compression. In addition, Sibson (1992, 2001) and Sibson et al. (1988) suggest these large cycles of fluid pressure are particularly important in the lower regions of what they call the 'seismogenic zone' at crustal depths of approximately 10–14 km, whereas the Indarama lode gold deposit is estimated to have formed at a depth of about 6 km (McKeagney, 1998) with reference to the crustal continuum model of lode gold deposits of Groves (1993).

Sibson (2001) notes that when present, low cohesion faults that are suitably orientated for reactivation (such as the veins at Indarama) limit the extent of fluid pressure build up and the amplitude of fluid pressure decreases accompanying rupture. The mechanism of fluid pressure cycling described by Sibson and co-workers probably did occur at Indarama, but was much less significant due to the low angle of the fault veins. However, the cycle of fluid pressure build up, failure, fluid pressure drop, and re-sealing by hydrothermal deposition, is apparent during vein formation at Indarama. The stresses acting on the fractures varied within

these cycles, and the cycles (and therefore stress conditions) were repeated several times.

6. Discussion

The R ratio theory has mainly been applied to dykes (Delaney et al., 1986; Baer et al., 1994; Jolly and Sanderson, 1995, 1997) and to ridge and fracture geometries at obliquely spreading mid-ocean ridges (Tuckwell et al., 1996; Abelson and Agnon, 1997) but so far has not been applied to veins or mineral deposits. The similarity in the processes of forming veins and dykes means that this technique, for obtaining relative magnitudes of stress and fluid pressure at the time of fracture opening, is valid.

The theory is based on an infinitely long plane within a homogenous medium. The veins at Indarama are in homogenous basalt, but the planes are not infinitely long; instead they are essentially long (tens to hundreds of metres), planar fractures, with only small-scale irregularities (centimetre and decimetre scales). Dilation can be created by the formation of rideover-type structures and dilational jogs along differently orientated sections of a fault and thereby provide zones of dilation by fault slip instead of by fluid pressure exceeding normal stress on the fractures (e.g. Hodgson, 1989). However the limited shear displacement along the lodes renders this mechanism inappropriate for Indarama. The size of the ellipse in Fig. 12d was determined by the range of pole orientations assumed to represent synchronously dilated fractures. Multiple phases of reactivation will cause superposition of the data, although, with all the data indicating broadly synchronous fracture reactivation, the dilation of the fractures and fluid flow are treated collectively as a single event. Repetitions of similar veining episodes and the consistent orientation of the oblate stress ellipsoid over a protracted time span permits the deformation controlling mineralisation to be considered as one, overall tectonic event.

Fracture initiation probably took place during several deformation episodes, resulting in a wide range of fracture orientations being present in the rock mass. The elongation of the cluster to vein-poles in the NE–SW direction and the constriction of the ellipse in the NW–SE direction (Fig. 12d) suggest that the principal stresses acting at the time of vein reactivation and fluid flow included a sub-horizontal, SSE–NNW-directed σ_1, a sub-horizontal, ENE–WSW-directed σ_2, and a sub-vertical σ_3. The relative magnitudes of the principal stresses indicate an oblate stress ellipsoid at the time of fluid flow and vein reactivation. The clustered nature of the poles to veins at Indarama suggests that the fluid pressure was greater than the minimum principal stress but less than the intermediate principal stress ($\sigma_3 < P_f < \sigma_2 < \sigma_1$). The internal structures of veins at Indarama are not complex and do not suggest significant re-orientation of the stress field during dilation. This oblate style of stress field, therefore, acted during repeated reactivation and fluid flow. Thus, broadly synchronous formation of the E–W- and N–S-dipping lodes, with many shared characteristics, can be readily explained in the stress field described above (Section 4.5). Compressional stress directions identified by (i) the Mohr circle analysis of relative magnitudes of stress and fluid pressure, and (ii) lode geometry and kinematics, and their compatibility with regional tectonics indicate synchronous sub-horizontal compression in both NNW–SSE and ENE–WSW directions. This deformation model, therefore, provides the tectonic constraints for the oblate stress ellipsoid that controlled the formation of the Indarama lodes.

7. Conclusions

Application of the 3-D Mohr circle technique to the Indarama veins has produced meaningful results that are consistent with interpretations and predictions on a variety of scales. The broad range of lode orientations, all at low to moderate dips, indicates a constrictional stress field, and the results of the driving pressure/stress ratio analysis show that the intermediate principal stress was approximately 67% of the maximum principal stress. The fairly narrow orientation range of veins able to dilate implies a fluid pressure less than the intermediate stress (σ_2) but greater than the minimum principal stress (σ_3).

The data have demonstrated that when hydrothermal fluid(s) exploited the fracture system at Indarama resulting in mineralisation, the dominant compressive stress was directed NNW–SSE. Previous workers studying gold metallogenesis in the region have emphasized that compression from the NE was the dominant tectonic control on the formation of gold deposits in the Midlands Greenstone Belt but had no constraining craton-wide tectonic model. An understanding of the distal effects of the Limpopo Orogen is clearly necessary if the structural controls on the formation of mineral deposits in central Zimbabwe are to be successfully interpreted. By applying a technique that emphasizes the relative magnitudes of stresses and fluid pressures, a more complete understanding of the stress field evolution has been achieved. This has highlighted the important role of NNW–SSE compression during the mineralisation event, which could not be ascertained from a study of the geometry of the lodes in the absence of a 3-D Mohr circle analysis.

This study clearly indicates that the convergence of the Zimbabwe craton with the Central Zone of the Limpopo Belt (Treloar and Blenkinsop, 1995) played a much more important and direct role in the formation of lode gold deposits in central Zimbabwe than previously thought. As a consequence, exploration for further gold-bearing lodes in the Midlands Greenstone Belt must take into consideration the geometry of geological structures generated and reactivated within the oblate stress field defined in this study.

Acknowledgements

Financial and logistic support of Pan Reef Mining (Pvt) Ltd, owners of the Indarama Mine at the time of the study, is gratefully acknowledged. S. Cox and an anonymous reviewer are thanked for their constructive comments.

References

Abelson, M., Agnon, A., 1997. Mechanisms of oblique spreading and ridge segmentation. Earth and Planetary Science Letters 148, 405–421.

Angelier, J., 1984. Tectonic analysis of fault slip data sets. Journal of Geophysical Research 89, 5835–5848.

Anhaeusser, C.R., 1976. The nature and distribution of Archaean gold mineralisation in Southern Africa. Mineral Science Engineering 8, 46–48.

Baer, G., Beyth, M., Reches, Z., 1994. Dikes emplaced into fractured basement, Timna Igneous Complex, Israel. Journal of Geophysical Research 99, 24039–24051.

Barton, C.A., Zoback, M.D., Moos, D., 1995. Fluid flow along potentially active faults in crystalline rock. Geology 23, 683–686.

Blenkinsop, T.G., Frei, R., 1997. Dating the intrusion of the Razi Granites, Zimbabwe: tectonic implications for the Northern Marginal Zone of the Limpopo Belt and the Zimbabwe craton. In: Conference Abstract Volume, Harare, Zimbabwe, Intraplate magmatism and tectonics of southern Africa, and the 17th Colloquium on African Geology, 4.

Blenkinsop, T., Martin, A., Jelsma, H.A., Vinyu, M.L., 1997. The Zimbabwe Craton. In: de Wit, M.J., Ashwall, L. (Eds.), Greenstone Belts. Oxford University Monograph on Geology and Geophysics 35, pp. 567–580.

Campbell, S.D.G., Pitfield, P.E.J., 1994. Structural controls of gold mineralisation in the Zimbabwe craton—exploration guidelines. Zimbabwe Geological Survey Bulletin 101, 270.

Cox, S.F., Knackstedt, M.A., Braun, J., 2001. Principles of structural control on permeability and fluid flow in hydrothermal systems. Society of Economic Geologists Reviews 14, 1–24.

Delaney, P.T., Pollard, D.D., Zioney, J.I., McKee, E.H., 1986. Field relations between dikes and joints: emplacement processes and palaeostress analysis. Journal of Geophysical Research 91 (B5), 4920–4938.

Dirks, P.H.G.M., Jelsma, H.A., 1998. Horizontal accretion and stabilization of the Archaean Zimbabwe craton. Geology 26, 11–14.

Foster, R.P., Fisher, N.J., Porter, C.W., Fabiani, W.M.B., Carter, A.H.C., 1991. The tectonic and magmatic framework of Archaean lode-gold mineralisation in the Midlands Greenstone Belt, Zimbabwe. In: Ladeira, E.A., (Ed.), Brazil Gold '91, pp. 359–366.

Groves, D.I., 1993. The crustal continuum model for late-Archaean lode-gold deposits of the Yilgarn Block, Western Australia. Mineralium Deposita 28, 366–374.

Hancock, P.L., 1985. Brittle microtectonics: principles and practice. Journal of Structural Geology 7, 437–457.

Harrison, N.M., 1970. The geology of the country around Que Que. Rhodesia Geological Survey Bulletin No. 67.

Herrington, R.J., 1995. Late Archaean structure and gold mineralisation in the Kadoma region of the Midlands Greenstone Belt, Zimbabwe. In: Coward, M.P., Ries, A.C. (Eds), Early Precambrian Processes, Geological Society Special Publication 95, pp. 53–65.

Hodgson, C.J., 1989. The structure of shear-related, vein-type gold deposits: a review. Ore Geology Reviews 4, 231–273.

Horstwood, M.S.A., Nesbitt, R.W., Noble, S.R., Wilson, J.F., 1999. U–Pb zircon evidence for an extensive early Archaean craton in Zimbabwe: a reassessment of the timing of craton formation, stabilization, and growth. Geology 27, 707–710.

Jaeger, J.C., Cook, N.G.W., 1979. Fundamentals of Rock Mechanics, 3rd ed, Chapman and Hall, 593pp.

Jolly, R.J.H., Sanderson, D.J., 1995. Variations in the form and distribution of dykes within the Mull swarm, Scotland. Journal of Structural Geology 17, 1543–1557.

Jolly, R.J.H., Sanderson, D.J., 1997. A Mohr circle reconstruction for the opening of a pre-existing fracture. Journal of Structural Geology 19, 887–892.

Jolly, R.J.H., Wei, L., Pine, R.J., 2000. Stress-sensitive fracture-flow modelling in fractured reservoirs. SPE 59042, 2000 SPE International Petroleum Conference and Exhibition in Mexico held in Villahermosa, Mexico, 1–3 February 2000.

Macgregor, A.M., 1932. The geology of the country around Que Que, Gwelo district, Southern Rhodesia. Geological Survey Bulletin No. 20.

Macgregor, A.M., 1951. Some milestones in the Precambrian of southern Rhodesia. Geological Society of South Africa Proceedings 54, 27–71.

Mardia, K.V., 1972. Statistics of Directional Data. Academic Press, London.

McKeagney, C.J., 1998. Structural and alteration characteristics of the Indarama lode gold deposit, Zimbabwe; implications for craton-wide tectonism and mineralisation. PhD thesis, University of Southampton, UK.

Means, W.D., 1976. Stress and Strain. Springer-Verlag, Berlin.

Nguyen, P.T., Cox, S.F., Harris, L.B., Powell, C.McA., 1998. Fault-valve behaviour in optimally oriented shear zones: an example at the Revenge gold mine, Kambalda, Western Australia. Journal of Structural Geology 20, 1625–1640.

Nisbet, E.G., Wilson, J.F., Bickle, M.J., 1981. The evolution of the Rhodesia craton and adjacent Archaean terrain: tectonic models. In: Kröner, A., (Ed.), Precambrian Plate Tectonics, pp. 161–183.

Phillips, W.J., 1972. Hydraulic fracturing and mineralization. Journal of the Geological Society, London 128, 337–359.

Porter, C.W., Foster, R.P., 1991. Multi-phase ductile–brittle deformation and the role of Archaean thrust tectonics in the evolution of the Globe and Phoenix gold deposit, Zimbabwe. In: Ladeira, E.A., (Ed.), Brazil Gold '91, pp. 665–671.

Sanderson, D.J., Zhang, X., 1999. Critical stress localisation of flow associated with deformation of well-fractured rock-masses, with implications for mineral deposits. Special Publication of the Geological Society of London 155, 69–81.

Sibson, R.H., 1985. A note on fault reactivation. Journal of Structural Geology 7, 751–754.

Sibson, R.H., 1992. Implications of fault-valve behaviour for rupture nucleation and recurrence. Tectonophysics 211, 283–293.

Sibson, R.H., 2001. Seismogenic framework for hydrothermal transport and ore deposition. Society of Economic Geologists Reviews 14, 25–50.

Sibson, R.H., Robert, F., Poulson, K.H., 1988. High-angle reverse faults, fluid-pressure cycling, and mesothermal gold-quartz deposits. Geology 16, 551–555.

Stowe, C.W., 1971. Summary of the tectonic development of the Rhodesian Archaean craton. Special Publications of the Geological Society of Australia 3, 377–383.

Stowe, C.W., 1980. Wrench tectonics in the Rhodesian Archaean craton. Transactions of the Geological Society of South Africa 83, 193–205.

Taylor, P.N., Kramers, J.D., Moorbath, S., Wilson, J.F., Orpen, J.L., Martin, A., 1991. Pb/Pb, Sm–Nd and Rb–Sr geochronology in the Archaean craton of Zimbabwe. Chemical Geology 87, 175–196.

Treloar, P.J., Blenkinsop, T.G., 1995. Archaean deformation patterns in Zimbabwe: true indicators of Tibetan-style crustal extrusion or not? In: Coward, M.P., Ries, A.C. (Eds.), Early Precambrian Processes. Geological Society Special Publication 95, pp. 87–108.

Tuckwell, G.W., Bull, J.M., Sanderson, D.J., 1996. Models of fracture orientation at oblique spreading centres. Journal of the Geological Society, London 153, 185–189.

Wilson, J.F., 1981. Zimbabwe. In: Hunter, D.R., (Ed.), Precambrian of the Southern Hemisphere, Developments in Precambrian Geology, Elsevier, pp. 454–488.

Wilson, J.F., 1990. A craton and its cracks: some of the behaviour of the Zimbabwe block from the late Archaean to the Mesozoic in response to horizontal movements, and the significance of some of its mafic dyke fracture patterns. Journal of African Earth Science 10, 483–501.

Wilson, J.F., Bickle, M.J., Hawkesworth, C.J., Martin, A., Nisbet, E.G., Orpen, J.L., 1978. Granite–greenstone terrains of the Rhodesian Archaean craton. Nature 271, 23–27.

Wilson, J.F., Nesbitt, R.W., Fanning C.M., 1995. Zircon geochronology of Archaean felsic sequences in the Zimbabwe craton: a revision of greenstone stratigraphy and a model for crustal growth. In: Coward, M.P., Ries, A.C. (Eds.), Early Precambrian Processes, Geological Society Special Publication 95, pp. 109–126.

Woodcock, N.H., Naylor, M.A., 1983. Randomness testing in three-dimensional orientation data. Journal of Structural Geology 5, 539–548.

Zhang, X., Sanderson, D.J., 1997. Effects of loading direction on localized flow in fractured rocks. In: Yuan, J.X., (Ed.), Computer Methods and Advances in Geomechanics, Balkema, Rotterdam, pp. 1027–1032.